Enhanced Photocatalytic Performance of CuFeO2-ZnO Heterostructures for Methylene Blue Degradation under Sunlight

Preethi Sudarsan (preethi.sp21@gmail.com)
Pondicherry University https://orcid.org/0000-0001-7643-5287
Vivek Seethapathy
Pondicherry University
Priya Ranganathan
University of Madras
Balakumar S
University of Madras
Suresh Babu Krishnamoorthy
Pondicherry University

Research Article

Keywords: Hydrothermal, Photocatalysis, methylene blue, sunlight, heterostructures

Posted Date: March 1st, 2021

DOI: https://doi.org/10.21203/rs.3.rs-231641/v1

Version of Record: A version of this preprint was published at Journal of Materials Science: Materials in Electronics on August 2nd, 2021. See the published version at https://doi.org/10.1007/s10854-021-06712-w.

Enhanced photocatalytic performance of $CuFeO_2$-ZnO heterostructures for methylene blue degradation under sunlight

S. Preethi [a], S.Vivek [a], R.Priya[b], S. Balakumar[b], K. Suresh Babu [a,*]

[a] Centre for Nanoscience and Technology, Madanjeet School of Green Energy Technologies, Pondicherry University (A Central University), Puducherry, 605014, India

[b] National Centre for Nanoscience and Nanotechnology, University of Madras, Tamilnadu, India.

* Corresponding Author

E mail: sureshbabu.nst@pondiuni.edu.in

Phone: +91-413-2654976

Abstract:

Development of heterostructures is one of the constructive strategies for enhancing the photocatalytic activity. Here, novel $CuFeO_2$-ZnO heterostructures with different weight percentage ($CuFeO_2$ = 0.5, 1, 5, 10%) were prepared by two-step precipitation-hydrothermal process. The structural confirmation was done by XRD and Raman analysis. The photocatalytic efficiency of the heterostructures was assessed by the degradation of methylene blue under sunlight. $CuFeO_2$-ZnO heterostructures enhanced the photocatalytic performance compared to pure ZnO and $CuFeO_2$. Among all, 5 wt % of $CuFeO_2$ on ZnO exhibited 100% degradation with 16 fold faster kinetics than ZnO. Time-resolved photoluminescent analysis revealed the increase in lifetime of charge carriers in the heterostructure. The band alignments of ZnO and $CuFeO_2$, evaluated by Mott–Schottky revealed the existence of Type 1 heterostructures. Further, the heterostructures exhibited good recyclability. Thus, the present work demonstrates the use of p-type $CuFeO_2$ and n-type ZnO heterostructures as potential photocatalysts.

Keywords: Hydrothermal; Photocatalysis; methylene blue; sunlight; heterostructures

Introduction

The increasing adverse effects of industrial pollution on humans and environment thrust the development of research on clean energy and environment. Hence, toxic-free removal of these large quantities of harmful industrial effluents is the need of the hour to obtain clean water. Presently, research on photocatalysis has been extensively explored for responding to environmental pollution. Several kinds of study on TiO_2 [1], ZnO [2], ZnS [3], CdS [4],CdSe, V_2O_5 [5], WO_3 [6], and Fe_2O_3 [7] have proven their usage for photocatalytic removal of organic azo dyes. Among all these, ZnO, the n-type semiconductor has picked up steam due to its low cost, easily controlled morphology, high redox potential, photonic and oxidation resistive and non-toxic nature. However, due to its wide bandgap (~3.2 eV), the optical absorption is constrained to UV region which is only 4% of the total sunlight radiation. This mitigates the use of naturally available sunlight as the source of energy. Further, in ZnO, the excited electron recombines with hole faster and decreases the free carrier concentration required for degradation, therefore hindering the photocatalytic performance [8]. To promote the absorption of these semiconductors in the visible region and to suppress the electron-hole recombination, researchers adopted several strategies such as introducing dopants [9,10], manoeuvring the size and shape of the photocatalytic materials [11,12], formation of heterojunctions. Among these, contriving the photocatalyst materials by forming heterojunctions with other semiconductor oxides would pave the way for enhanced photocatalytic activity by forming an interfacial electric field which would effectively separate the charge-carriers. Meng et al. identified an enhanced photocatalytic CO_2 reduction by $Ni(OH)_2/TiO_2$ [13]. $AgI/BiVO_4$ has shown 43% higher photocatalytic activity compared to $BiVO_4$ [14]. Jiang et al. developed TiO_2-ZnO heterojunctions for decolourisation of C.I. Basic Blue 41 [15]. Udin et al. reported enhanced photocatalytic activity for SnO_2–ZnO heterostructure towards methylene blue degradation [16]. Among many heterojunctions viz. metal-semiconductor, semiconductor-semiconductor

(p-p type, p-n type, n-n type), p-n heterojunctions have shown to be favouring effective charge separation, longer lifetime and rapid charge transfer. CuO -ZnO p-n type heterostructure has shown better performance for gas sensing and photocatalytic degradation [17,18,19]. Shaheer et al. reported that reduced GO supported TiO_2-$In_{0.5}WO_3$ showing a 12 fold improvement in comparison to bare TiO_2[20]. Similarly, ZnO-CdS, ZnO-ZnS, ZnO-CuO, ZnO-GaN heterostructures have shown increased performance in comparison to pristine ZnO. ZnOSe/ZnO/boron doped ZnO exhibited reduced electron-hole recombination rate compared to pristine ZnO. ZnO/$NiFe_2O_4$ nanocomposite exhibited enhanced degradation efficiency compared to ZnO [21]. Further to enhance the visible light-harvesting, heterojunction formation with narrow bandgap semiconductors has found to be advantageous. Recently p-type delafossite materials such as $CuAlO_2$, $CuFeO_2$ have received considerable attraction as photocathodes for photoelectrochemical water splitting and hydrogen evolution reaction and as transparent conducting oxides [22,23]. In particular, $CuFeO_2$ delafossite has drawn great attention due to its absorption in the visible region with a narrow bandgap energy of ~1.5 eV. But it suffers meagre transport properties due to higher electron-hole recombination rate.

Hence, to address these challenges, we report the construction of heterostructure between a p-type narrow bandgap ($CuFeO_2$) and n-type wide bandgap semiconductor (ZnO) for improved methylene blue degradation and the results have been correlated to the physical-chemical properties of the material. Thus this paper would provide a scientific outlook to further design novel heterostructures for enhanced solar harvesting.

Experimental procedure

Synthesis of pure ZnO

Zinc oxide (ZnO) was synthesised by precipitation method using zinc nitrate hexahydrate ($Zn(NO_3)_2 \cdot 6H_2O$, Himedia) and sodium hydroxide (NaOH, Himedia) as precursors. 14 g of

zinc nitrate was dissolved in distilled water. To this, 3M NaOH was added to maintain the pH of 11. The resultant solution was stirred for 12 hours forming a precipitate. Then the precipitate was centrifuged and dried at 80 °C overnight. The dried powder was calcined at a temperature of 500 °C for 4 hours.

Synthesis of pure $CuFeO_2$

$CuFeO_2$ (CFO) was synthesised by hydrothermal method. An aqueous solution of copper ($Cu(NO_3)_2.6H_2O$, Himedia and iron nitrates ($Fe(NO_3)_3.9H_2O$, Himedia) was prepared by dissolving in stoichiometric ratio. To this, 3M NaOH was added to achieve a pH of 14. The solution was stirred for 30 minutes, then 1 ml of hydrazine hydrate was added to the mixture. Then the solution was decanted to a Teflon vessel which was later autoclaved at 180 °C for 24 hours. After this process, the sample was washed 3 times, two times with double distilled water and once with ethanol. The resultant nanopowder was collected after drying at 80 °C overnight.

Synthesis of $CuFeO_2$-ZnO

Different weight ratios of $CuFeO_2$-ZnO (xCF-ZnO, x= 0.5, 1, 5, 10%) p-n heterostructures were synthesized by hydrothermal method. The calcined ZnO was dispersed in distilled water, and then the stoichiometric amount of the nitrates of Cu and Fe were added. Then, NaOH and hydrazine hydrate was added similarly followed for the $CuFeO_2$.

Characterization

The phase analysis was done using X-ray diffractometer (Rigaku, Ultima IV) with Cu K_α radiation (λ=1.5406 Å) at a scan rate of 0.02° per second in the 2θ range between 20 and 80°. The Raman spectra were obtained by Renishaw, RM 2000 with a laser excitation wavelength of 785 nm and 0.3 mW power. The morphological characterization was done using a Scanning Electron Microscope (Hitachi, Model-S-34000N). The optical analysis was carried UV-Vis spectrophotometer (Shimadzu, UV- 3600). Time-resolved photoluminescence (TRPL)

analysis was done using fluorescence lifetime spectrometer (Jobin Yvon, FLUOROLOG-FL3-11). The electrochemical analysis was done using PARSTAT 4000A potentiostat. Mott Schottky and electrochemical impedance analysis of the heterostructures were carried out using a three-electrode cell consisting of Ag/AgCl as reference electrode and platinum as counter electrode.

Results and discussion

X-Ray Diffraction

Phase identification of the samples was done by X-ray diffraction analysis. Fig. 1 shows the XRD pattern of pristine ZnO, $CuFeO_2$ and xCF-ZnO (x= 0.5,1, 5 and 10). All the peaks were sharp, indicating the crystalline structure of all the prepared samples. The diffraction peaks at 2Θ= 31.6°, 34.5°, 36.2°, 47.6°, 56.7°, 62.9°, 66.4°, 67.9° and 69.1° corresponds to the (100), (002), (101), (102), (110), (103), (200), (112) and (201) crystal planes, respectively, of hexagonal wurtzite structure of ZnO with space group $P6_3mc$ (JCPDS: 36-1451). Diffraction peaks at 31.2°, 34.5°, 35.7°, 40.2°, 55.2, 61.3°, 64.7°, 70.2° in CFO can be ascribed to (006), (101), (012), (104), (018), (110), (010) and (011) crystal planes of pure rhombohedral delafossite $CuFeO_2$ with the R3m space group (JCPDS: 39-0246).

In 0.5 and 1CF-ZnO, no peak other than corresponding to ZnO was observed. But in 5 and 10 CF-ZnO, besides diffraction peaks of ZnO, additional peaks were observed at 35.3° and 40.7° (denoted by arrow) which are characteristic of $CuFeO_2$. This substantiates the presence of both ZnO and $CuFeO_2$. The peaks other than (012) and (104) are not distinct due to the low scattering ability of CFO on ZnO. The absence of peaks specific to $CuFeO_2$ in xCF-ZnO ($x<5$) is due to the low concentration of $CuFeO_2$ which might be below the XRD detection limit. No additional peak implies the purity of the synthesised material. The calculated lattice parameter of ZnO was found to be a, b = 0.3348 nm, c = 0.569 nm and CFO was a = b = 0.304 nm,

c=1.702 nm. No peak shift was observed in xCF-ZnO and the lattice parameter of ZnO remained constant substantiating the successful formation of heterostructure without doping.

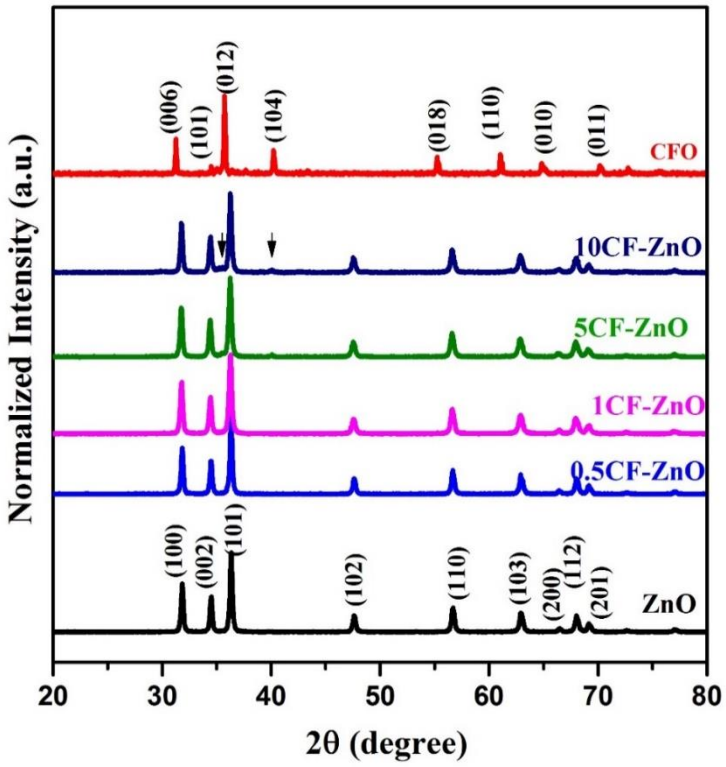

Fig. 1 XRD pattern of pure ZnO, xCF-ZnO(x=0.5,1,5,10) and pure CFO. The peaks marked with arrow corresponds to $CuFeO_2$

The crystallite size of the synthesised sample was computed by Debye-Scherer's formula. The crystallite size of ZnO (29.6 ± 2 nm) did not vary since ZnO was first synthesised using precipitation method and then hydrothermally treated to form a p-n heterostructure. This denotes that the hydrothermal condition did not affect the previously synthesised ZnO. The crystallite size of CFO was calculated to be 41.2± 3 nm, while that of 10CF-ZnO was calculated to be 18± 2 nm. The decreased crystallite size in the composite is due to the hindrance in the nucleation of the host structure ($CuFeO_2$) in the presence of foreign ZnO.

Raman spectroscopy

The vibrational properties of the heterostructures were examined by Raman spectroscopy. Fig. 2 depicts the Raman spectra of xCF- ZnO system. As per group theory, the optical modes present in a wurtzite ZnO are given in equation (1)

$$\Gamma opt = A_1 + 2B_2 + E_1 + 2E_2 \quad (1)$$

where A_1 and E_1 are active modes which are further divided into longitudinal optical (A_1 LO and E_1 LO) and transverse optical (A_1 TO and E_1 TO) modes. In this, A_1, E_1 and E_2 represents Raman-active modes while B_2 are Raman inactive modes.

The prominent peak at 436 cm^{-1} corresponds to the E_2 mode of vibration in ZnO lattice which

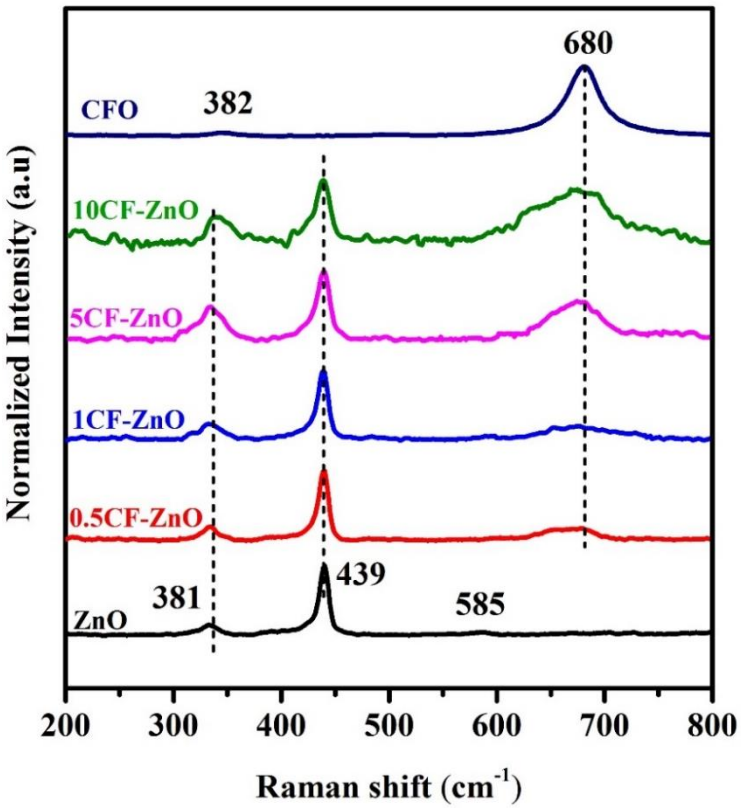

Fig. 2 Raman spectra of ZnO, CFO and xCF-ZnO system

represents the parallel vibration of paired Zn and O atom in the same direction. Besides the E_2 band, the small intense peaks at 381 and 585 cm^{-1} is accredited to A_1 (TO) mode and A_1(LO)/E_1(LO), respectively. The peak at 332 is due to the multi phonon scattering modes that can be assigned to the optical phonon overtone with A_1 symmetry [24]. $CuFeO_2$ delafossite with rhombohedral structure contains twelve vibrational modes at the zone centre, represented as

$$\Gamma opt = A_{1g} + E_g + 3A_{2u} + 3E_u. \quad (2)$$

Where subscript g represents Raman active modes, subscript u denotes the infrared active modes. CFO exhibits A_{1g} and E_g mode of vibrations at 680 and 382 cm^{-1}, respectively. In xCF-ZnO system, the peak at 680 cm^{-1} emerges with the increase in concentration from 0.5 to 10CF-ZnO, which is characteristic to the vibration of rhombohedral $CuFeO_2$. Further, no shift in the representative peaks of CFO and ZnO was observed denoting the absence of Cu or Fe in ZnO lattice.

Morphological study

The surface morphology of the heterostructure was inspected by scanning electron microscope. Fig. 3 depicts the SEM images of 0.5CF-ZnO and 5CF-ZnO. The heterostructure exhibits spherical morphology. The average particle size was acquired by calculating the particle size of around 100 particles. Inset represents the histogram of particle size distribution. The histogram exhibited lognormal distribution with a mean particle size of 113 and 119nm for 0.5CF-ZnO and 5CF-ZnO, respectively. The samples exhibited separate particles projecting the homogeneity of the samples. Further, no change in the morphology of ZnO occurred upon forming CF-ZnO heterostructure.

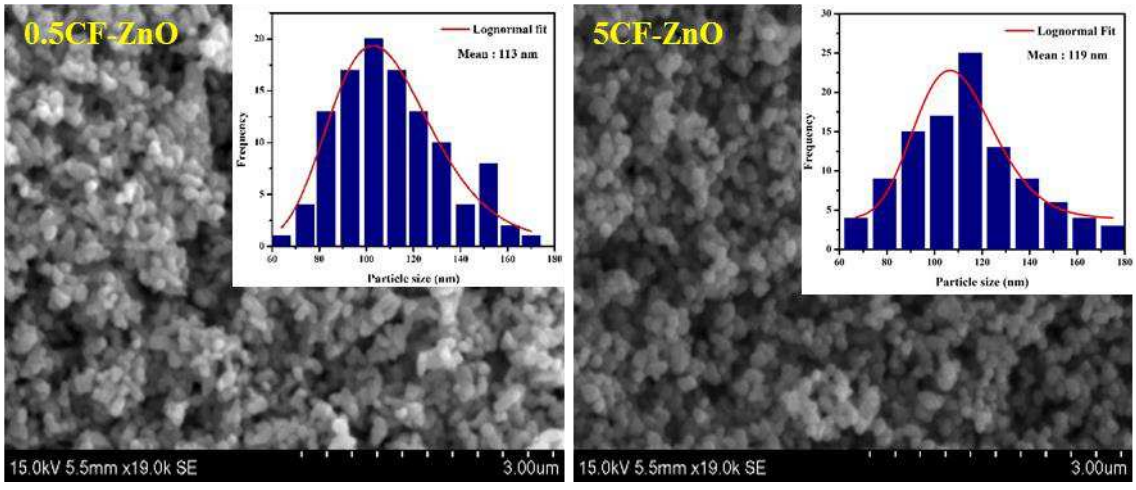

Fig. 3 SEM images of 0.5CF-ZnO and 5CF-ZnO

Optical analysis

The optical absorption of the heterostructures was inspected to find the bandgap of the samples. Fig. 4 depicts the absorption spectra of the CF-ZnO system in the UV-Vis region. ZnO absorbs only in the UV region (200-400 nm). The band at 354 nm is attributed to the bandgap excitonic absorption. In CFO, strong absorption in UV region (200-240 nm) was found as well as in the visible region.

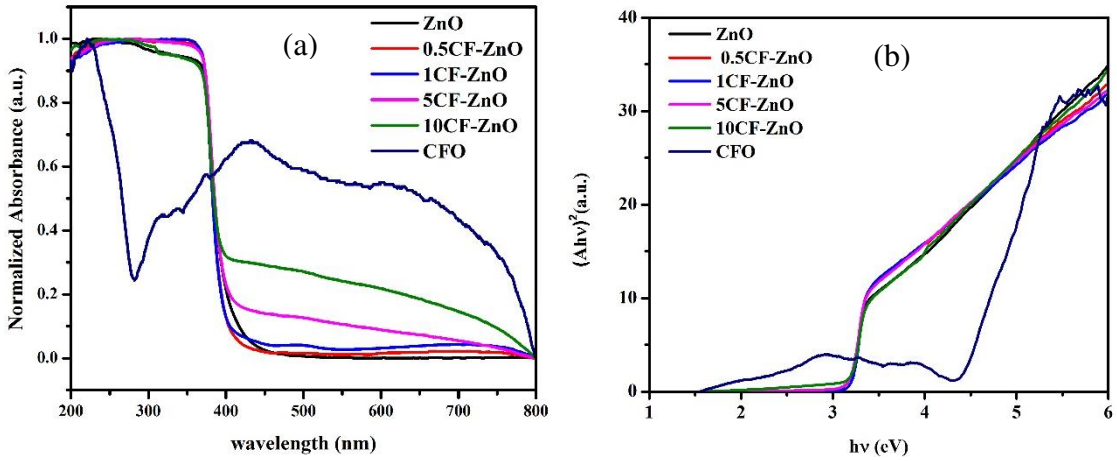

Fig. 4 Absorbance spectra (a) Tau plot (b) of the xCF-ZnO system

The absorption peak between 200-240 nm in CFO is due to the charge transfer excitation from the valence band to the conduction band [25]. In comparison to ZnO, it can be observed that with an increase in wt% of CFO in ZnO, the optical absorption in visible region increases. This indicates the enhanced solar light harvesting property upon forming ZnO-CFO heterostructures compared to pure ZnO which is essential for enhancing the photocatalytic performance. Both ZnO and CFO being indirect semiconductors, the bandgap energy was obtained using equation 3

$$(\alpha h\nu)^2 = A(h\nu - E_g) \qquad (3)$$

where, α, h, ν, A, and E_g are the absorption coefficient, Planck constant, frequency, constant and bandgap, respectively. Extrapolating the plot of $[\alpha h\nu]^2$ vs. the energy to x –axis provides the bandgap. The bandgap values were found to be 3.15, 3.19, 3.17, 3.12, 3.11 and

1.5eV for ZnO, 0.5, 1, 5, 10 CF-ZnO and CFO, respectively. ZnO with bandgap 3.15eV absorbs visible light scarcely. But CFO nanoparticles strongly absorb visible light due to their narrow bandgap. Thus combining these two materials would improve the visible light absorption without any change in bandgap.

Photocatalytic activity

The photocatalytic activity of xCF-ZnO heterostructures was evaluated by the photodegradation of methylene blue under sunlight. 20 mg of the xCF-ZnO heterostructures was added to 50 ml of methylene blue dye solution with a concentration of 10mg/L. The combined solution of the respective photocatalyst and dye was stirred in dark for 30 min to achieve the adsorption-desorption equilibrium. Then, the reactant solution was exposed to sunlight for 60 min. The intensity of the sunlight was noted using a lux meter (85000 lux). The latitude and longitude coordinates were 12° 0' 56.967" N and 79° 51' 8.978" E. 1 ml of the exposed solution was collected at an interval of every 10 min, subsequently centrifuged and was analyzed by UV−Vis spectrophotometer. Fig. 5 shows the UV-Vis absorption spectra for MB degradation by the prepared heterostructures at an interval of 10 min. The degradation efficiency of the respective photocatalysts was evaluated from the UV-Vis spectra using equation 4,

$$\eta\ (\%) = \frac{C_0 - C}{C_0} \qquad (4)$$

where, C_0 is the initial concentration at 0 min and final concentration of the dye at 60 min. Fig. 6a represents the bar diagram of the degradation efficiency of pure ZnO, CFO and CF-ZnO heterostructures. Pristine ZnO showed only 38% degradation of methylene blue at 30 min while xCF-ZnO heterostructures showed enhanced degradation efficiency. 5CF-ZnO exhibited 100 % photodegradation in 30 minutes.

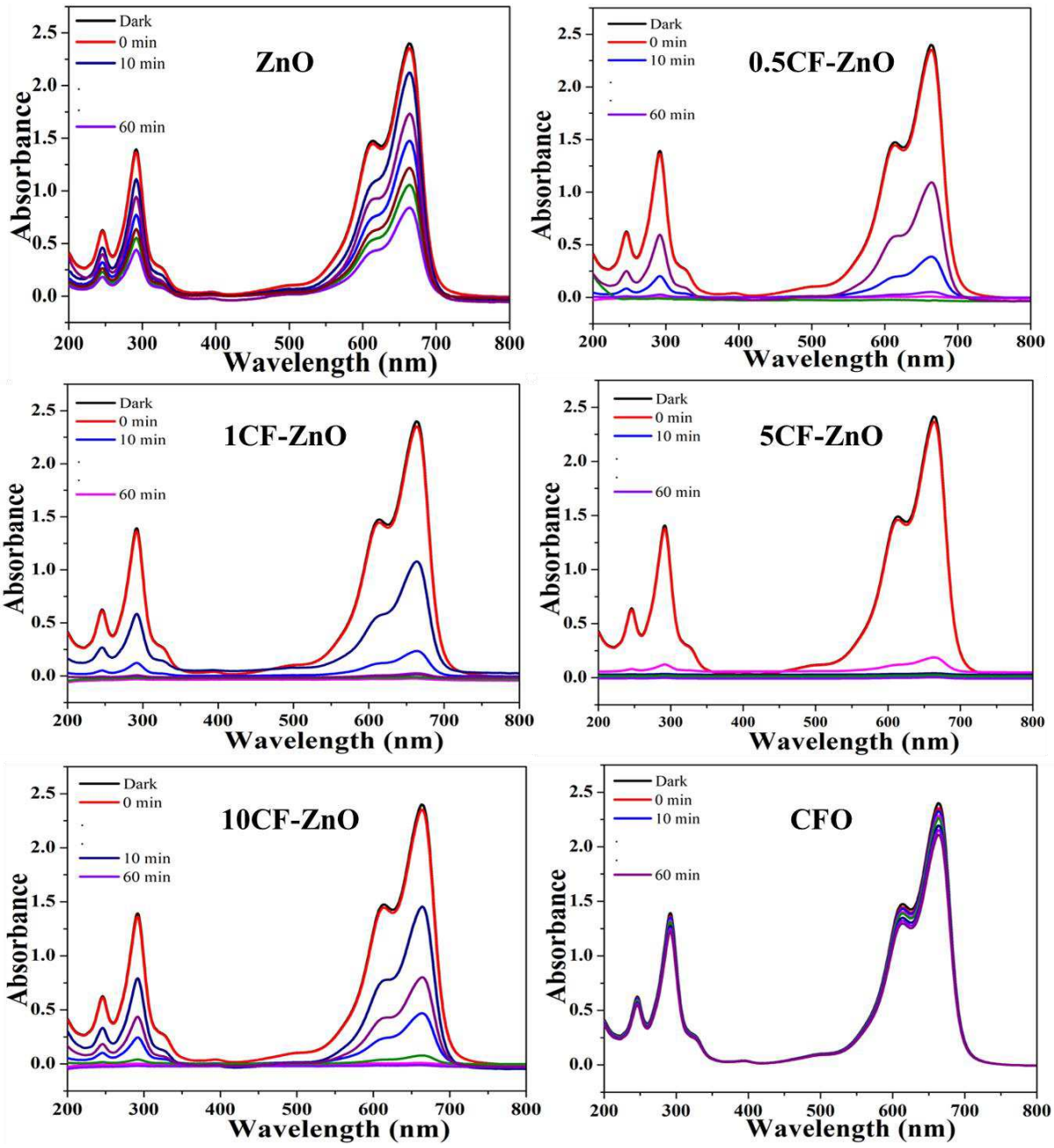

Fig. 5 Absorption spectra for the degradation of methylene blue by sunlight for ZnO and xCF-ZnO system

The increased photocatalytic ability of xCF-ZnO can be attributed to the combined effect of CFO and ZnO. The reaction kinetics for methylene blue degradation was quantified to compare the photocatalytic activity. The reaction exhibited pseudo-first-order kinetics and the rate constant is calculated using equation 4.

$$C = C_0 \exp(-kt) \qquad (4)$$

where, k is the rate constant and C is the concentration of the dye at different time intervals.

Table 1 displays the rate constant of the prepared catalyst for MB degradation. It is obvious from the table that all xCF-ZnO heterostructures showed higher rate constant compared to their pristine counterparts. 5CF-ZnO showed the highest rate constant value of 0.272 min^{-1} among all the samples.

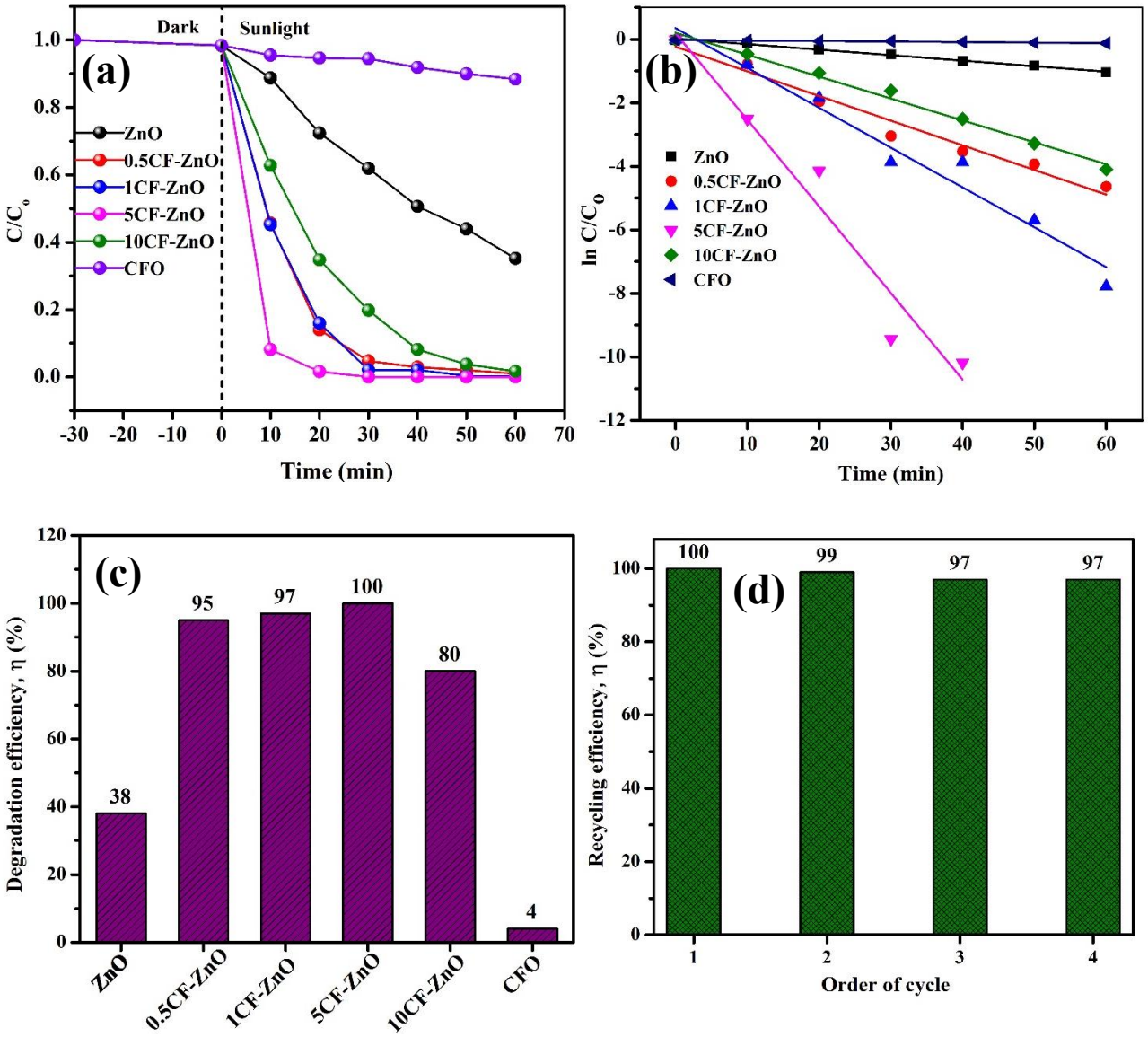

Fig. 6 a) Concentration vs irradiation time profile b) Reaction kinetics c) degradation efficiency at 30 min of ZnO and xCF-ZnO system for the degradation of methylene blue d) degradation efficiency of 5CF-ZnO for consecutive 4 cycles at 30 min

Table 1: Rate constant of the samples

S. No.	Sample Code	Rate Constant (min^{-1})
1	ZnO	0.017± 0.002
2	0.5CF-ZnO	0.077± 0.001
3	1CF-ZnO	0.125± 0.002
4	5CF-ZnO	0.272± 0.002
5	10CF-ZnO	0.068± 0.003
6	CFO	0.002± 0.001

The recyclability of the heterostructure was evaluated by sequentially retrieving the sample by centrifuging and drying at 60 °C for 1 hour after every degradation experiment. 5CF-ZnO was tested for recyclability and Fig. S1 shows the UV-Vis absorption spectra for the degradation of methylene blue from 2^{nd} to 4^{th} consecutive cycles. Fig. 6d shows the degradation efficiency for 4 consecutive cycles. The degradation reduced only by 3% which might be due to the weight loss of samples during the recovery process. Thus, the prepared heterostructure showed excellent stable performance. The basis for this enhanced photocatalytic activity by CF-ZnO heterostructures is validated by the time resolve photoluminescent study and electrochemical impedance spectroscopic analysis.(Section 3.6)

Photocatalytic Mechanism

Time-Resolved Photoluminescence Analysis

To proclaim the constructive effect of heterostructure formation on the photocatalytic performance, the lifetime of the excited charge carriers was measured by TRPL study. The samples were excited at 325 nm and the photoluminescence decay was monitored at 400 nm. Fig. 5 depicts the TRPL decay curves for xCF-ZnO heterostructures. ZnO exhibits a

multiexponential decay process and was fitted using bi-exponential model as represented in equation 4 to obtain two decay times τ_1 and τ_2.

$$R(t) = A_1 e^{\frac{-t}{\tau 1}} + A_2 e^{\frac{-t}{\tau 2}} \quad (4)$$

where, A_1 and A_2 represent the amplitude. τ_1 signifies the time constant for short decay process generated due to quasi-free excitons and τ_2 signifies the time for long decay process which is characteristic to localised exciton recombination [26].

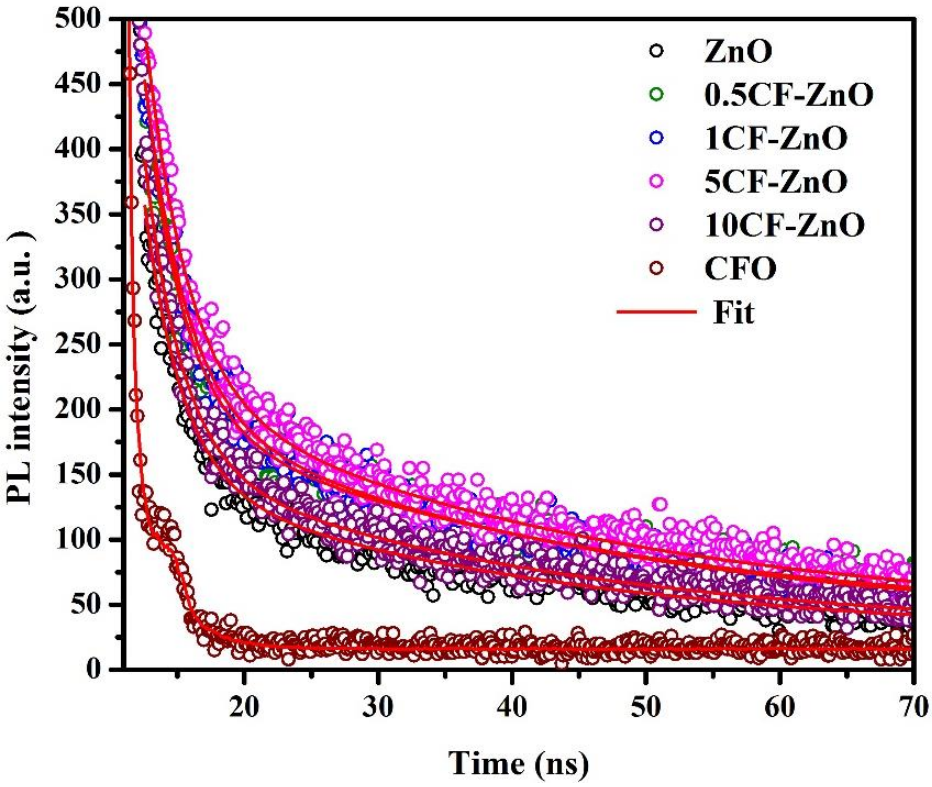

Fig. 5 Time resolved photoluminescent decay of pure ZnO,CFO and xCF-ZnO heterostructures

The average lifetime (τ_{avg}) of the charge carriers were calculated from the fitted values using equation 5 and are represented in Table 1.

$$t_{av} = = \frac{A_1 * {\tau_1}^2 + A_2 * {\tau_2}^2}{A_1 * \tau_1 + A_2 * \tau_2} \quad (5)$$

From Table 1, it could be observed that long lifetime increased from 29.6 ns in ZnO 33.4 ns in 5CF-ZnO. The lifetime increased with increase in weight percentage of $CuFeO_2$ in ZnO upto 5% farther on decreased in 10CF-ZnO. 5CF-ZnO exhibited a pronounced increase in average lifetime of 32.3 ns while that of ZnO was only 27.6 ns. This substantiates that the recombination of photogenerated electron –holes is suppressed in xCF-ZnO heterostructures leading to enhanced photocatalytic performance.

Table 2: Fitted values of amplitude and time constant obtained from TRPL decay curves and the calculated average life time of charge carriers

S.No	Sample Code	A_1 (%)	A_2 (%)	τ_1 (ns)	τ_2 (ns)	t_{av} (ns)
1	ZnO	45.5	54.5	2.78	29.6	27.6
2	0.5CF-ZnO	29.9	70.1	3.02	31.7	22.5
3	1CF-ZnO	30.4	69.6	3.06	32.0	23.6
4	5CF-ZnO	30.1	69.9	2.93	33.4	32.3
5	10CF-ZnO	42.8	60.2	2.81	30.6	28.9
6	CFO	27.9	97.21	0.2	2.69	0.85

Electrochemical Impedance spectroscopy

To explore the charge transfer dynamics of the heterostructures for the enhanced photocatalytic activity, the electrochemical analysis was done. Fig. 6 shows the Nyquist plot of xCF-ZnO the samples. The charge transfer resistance is calculated by fitting the Nyquist plot using an equivalent circuit consisting of resistor R_1 in series with $R_{CT}\|CPE$, where R_1 is the solution resistance and R_{CT} is the charge transfer resistance and CFE denotes the constant phase element. The calculated R_{CT} values for ZnO, 0.5CF-ZnO, 1CF-ZnO, 5CF-ZnO, 10CF-ZnO and CFO are 70, 33, 29, 19, 42 and 180 kΩ, respectively. This clearly depicts that the formation of

CF-ZnO heterostructure mitigated the charge transfer resistance which implies faster transfer of photogenerated charge carriers between n-type ZnO and p-type CFO.

Mott-Schottky analysis was done to probe the alignment of band structure in CFO and ZnO. The relative position of the valence band and the conduction band of ZnO, $CuFeO_2$ were evaluated from the flat band potential (V_{fb}) and the bandgap values. Fig. 7 depicts the Mott–Schottky (M–S) curves of CFO and ZnO. A positive/negative slope indicates that the CFO/ZnO is an n-type/p-type and affirms that electrons/holes are the majority of the charge carriers. V_{fb} was obtained by extrapolating the plot of $1/C^2$ vs potential to X-axis. The flat band potential of

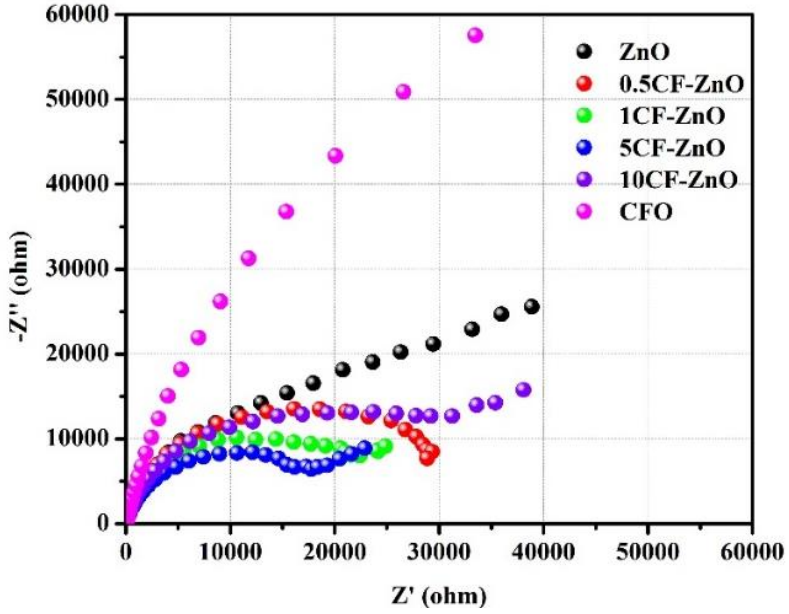

Fig. 6 Nyquist plot and Mott Schottky plot of xCF-ZnO system

ZnO and $CuFeO_2$ was calculated to be -0.82 and 1.17 eV vs Ag/AgCl, respectively. It is well known from literature, that the difference between the flat-band potential and the bottom/top edge of the conduction/valence band is negligible for an-type/p-type material [27]. Hence, we assume the value of flat band potential as the conduction/ valence band edge for n and p-type semiconductor, respectively. The band structure alignment between ZnO and CFO identified using flat-band potentials and bandgap energy using equation 6.

$$E_{CB} = E_{VB} - E_g \qquad (6)$$

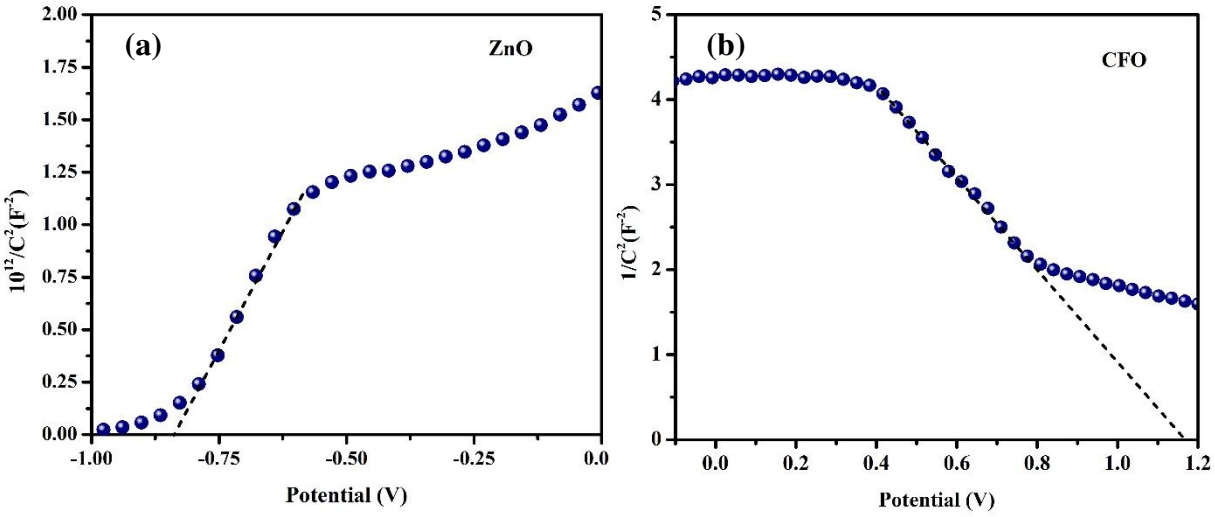

Fig. 7 Mott-Schottky plots of (a) ZnO and (b) $CuFeO_2$.

According to the calculated values of energy bands, the photocatalytic degradation mechanism of CF-ZnO heterostructures was proposed as shown in Fig. 8. The energy levels of CFO lies within the energy levels of ZnO forming a Type 1 Straddling type p-n heterostructure. After the contact formation, the energy levels of $CuFeO_2$ shifts upwards while the energy levels of ZnO are shifted downwards until the Fermi levels of CFO and ZnO forms an equilibrium. This results in the conduction band edge of CFO higher than ZnO. In consequence, an inner electric field is formed between the p-CFO and n-ZnO with minority charge carriers. When exposed to sunlight, CFO and ZnO absorbs photons and generate electron-hole pairs. The excited electrons migrate from the conduction band of CFO to the surface of ZnO across the interface. Simultaneously, the holes are transferred from the valence band of ZnO to CFO due to the more negative VB potential of CFO than that of the ZnO. This transfer of h^+ and e^- in the opposite direction increases the lifetime of photo-generated charge carriers in the heterostructures. The oxygen dissolved in the aqueous solution adsorb on the surface of the photocatalyst and react with these excited electrons and generate active free radical $^{\bullet}O_2$. Simultaneously, the holes react with H_2O to produce $^{\bullet}OH$ free radicals. This effectuates the degradation of methylene blue which are adsorbed on the surface of the photocatalyst by the

free radicals. Thus the formation of CF-ZnO heterostructure promoted faster transfer of electrons and holes between ZnO and CFO and subsequently hindered the recombination of photon generated electrons and holes, thereby enhancing the photocatalytic degradation.

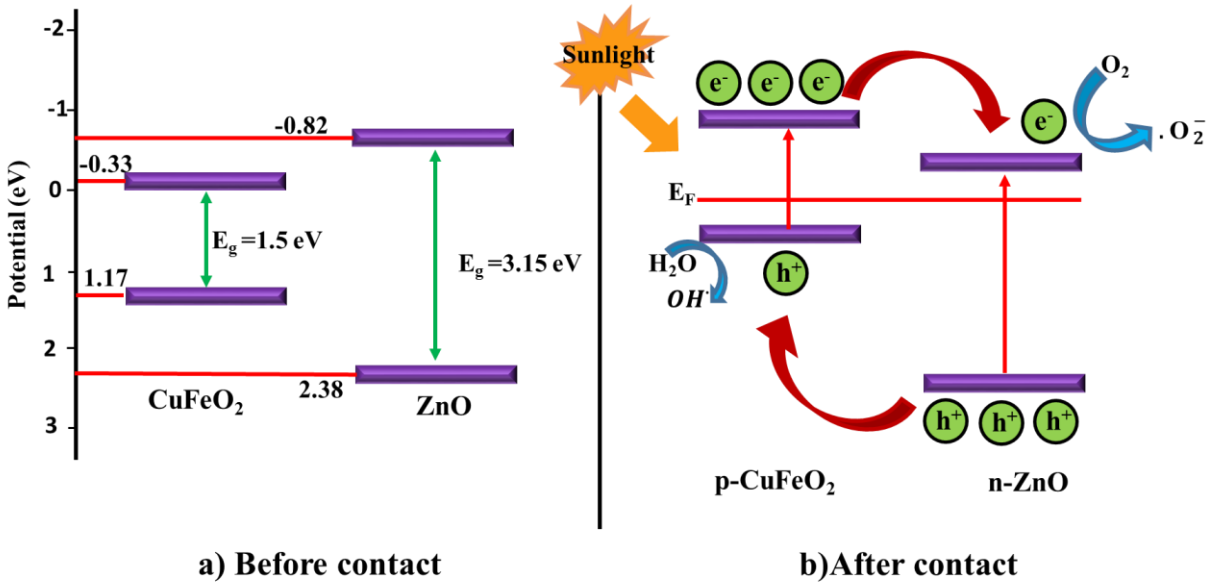

Fig. 8 Schematic diagram for the photocatalytic mechanism of CF-ZnO heterostructures

Conclusion

The present study focuses on developing novel p-n $CuFeO_2$-ZnO heterostructure by two- step precipitation – hydrothermal method. The weight ratios of p-$CuFeO_2$ and n-ZnO has a crucial role to control the photocatalytic property. A 16 fold increase in rate constant was observed for 5 CF-ZnO compared to ZnO for the photodegradation of methylene blue. TRPL study identified the increase in lifetime of charge carriers in the heterostructure. Flat band potential identification by Mott-Schottky analysis revealed the formation of Type 1 p-n heterostructure. Further electrochemical analysis validates faster charge transfer occurred in 5 wt% $CuFeO_2$-ZnO with lower charge transfer resistance. It could be identified from the results that the proposed p-n junction engineering of $CuFeO_2$-ZnO enhanced the photodegradation of methylene blue by enhanced visible light absorption, lowered charge transfer resistance and

charge carrier recombination. Overall, this strategy of creating p-n heterostructure would pave the way for developing other efficient solar harvesting devices.

Declarations

Funding: The authors acknowledge the funding from DST-SERB (EMR/2016/007577). Two of the authors, Dr.S.Preethi and Dr.S.Vivek thank the CSIR for Research Associateship and Senior Research Fellowship, respectively.

Conflicts of interest: The authors declare no conflict of interest.

References:

[1] K. Nakata, A. Fujishima, *J.Photochem. Photobio.C: Photochem.Rev.* 13, 169-189 (2012).

[2] S. Bhatia, N.Verma, *Mater.Res.Bull.* 95, 468-476 (2017).

[3] M. Hojamberdiev, B.Czech, A. C.Göktaş, K.Yubuta, Z.C.Kadirova, *J. Alloys Compd.* 827, 154339 (2020).

[4] L. Cheng, Q,Xiang, Y, Liao , H. Zhang, *Energy Environ. Sci.* 11, 1362-1391 (2018).

[5] S. K. Jayaraj, P. Thangadurai, *J. Mol. Liq.* 319, 114368 (2020).

[6] X. Liu, H. Zhai, P. Wang, Q.Zhang, Z. Wang, Y. Liu, Y. Dai, B. Huang, X. Qin and X.Zhang, *Catal. Sci. Technol.* 9, 652-658 (2019)

[7] C.N.C. Hitam, A.A.Jalil, *J. Environ. Manage*. 258, 110050 (2020).

[8] C.B. Ong, L. Y. Ng, A.W. Mohammad, Renewable *Sustainable Energy Rev.* 81, 536-551. (2019)

[9] D.M. Song, J.C. Li, *Comput. Mater. Sc*i. 65,175–81 (2012).

[10] M. Ahmad, E. Ahmed, Y. Zhang, N.R. Khalid, J. Xu, M. Ullah, *Curr. Appl.Phys.* 103, 13, 697–704 (2013).

[11] S.M. Ng, D.S.N. Wong, J.H.C. Phung, H.S. Chua. *Talanta* 116, 514–519 (2013).

[12] L. Qi, H. Li, L. Dong, *Mater. Lett.* 107, 354-356 (2013).

[13] A.Meng, S. Wu, B. Cheng, J. Yu , J.Xu, *J. Mater. Chem. A* 6, 4729-4736 (2018).

[14] S. K.Lakhera, R.Venkataramana, G. Mathew, H.Y.Hafeez, B. Neppolian, *Mater. Sci. Semicond. Process.* 106, 104756 (2020).

[15] Y. Jiang, Y.Sun, H. Liu, F. Zhu, H. Yin, Dyes Pigm. 78, 77-83 (2008).

[16] Md. T. Uddin, Y. Nicolas,C. Olivier,T. Toupance, L. Servant,M. M. Müller, H.-J. Kleebe, J.Ziegler, W. Jaegermann, *Inorg. Chem.* 51, 7764-7773(2012).

[17] M. Mansournia, L. Ghaderi, *J. Alloys Compds.* 691,171-177 (2017).

[18] S. Mridha, D. Basak, *Semicond. Sci. Technol.* 21, 928-9320 (2006).

[19] P. Sathishkumar, R. Sweena, J. J. Wu. S. Anandan, *Chem.Eng. J.* 171, 136-140 (2011).

[20] A.R. M. Shaheer, V.Vinesh, S. K.Lakher, B. Neppolian, *Sol.Energy* 213, 260-270 (2021).

[21] J.T. Adeleke, T. Theivasanthi, M. Thiruppathi, M. Swaminathan, T. Akomolafe, A.B. Alab, *Appl. Surf. Sci.* 455, 195–200 (2018).

[22] C.G. Read, Y. Park, K.S. Choi, *J. Phys. Chem. Lett.* 14, 1872-1876 (2012).

[23] M. S. Prévot, N. Guijarro, K. Sivula*, Chem. Sus. Chem.* 8, 1359-1367 (2015).

[24] R. Zhang, P.-G. Yin, N. Wang, L.Guo, *Solid State Sci*. 11,865–869 (2009).

[25] L. Naka-in, T. Kamwanna, P. Srepusharawoot, S. Pinitsoontorn, V.Amornkitbamrung, *Jpn J. Appl. Phys.* 54, 04DH10n(2015).

[26] B. Tian, B.J. Yang, J. Li, Z. Li, W.L. Zhen, Y.Q. Wu, G.X. Lu, *J. Catal.* 350, 189- 196 (2017).

[27] T. Jiang, Y. Zhao, H. Xue, *J. Mater. Sci.* 54, 11951–11958 (2019).

Supplementary Information

Enhanced photocatalytic performance of $CuFeO_2$-ZnO heterostructures for methylene blue degradation under sunlight

S. Preethi [a], S.Vivek [a], R.Priya[b], S. Balakumar[b], K. Suresh Babu [a,*]

[a] Centre for Nanoscience and Technology, Madanjeet School of Green Energy Technologies, Pondicherry University (A Central University), Puducherry, 605014, India

[b] National Centre for Nanoscience and Nanotechnology, University of Madras, Tamilnadu, India.

* Corresponding Author

E mail: sureshbabu.nst@pondiuni.edu.in

Phone: +91-413-2654976

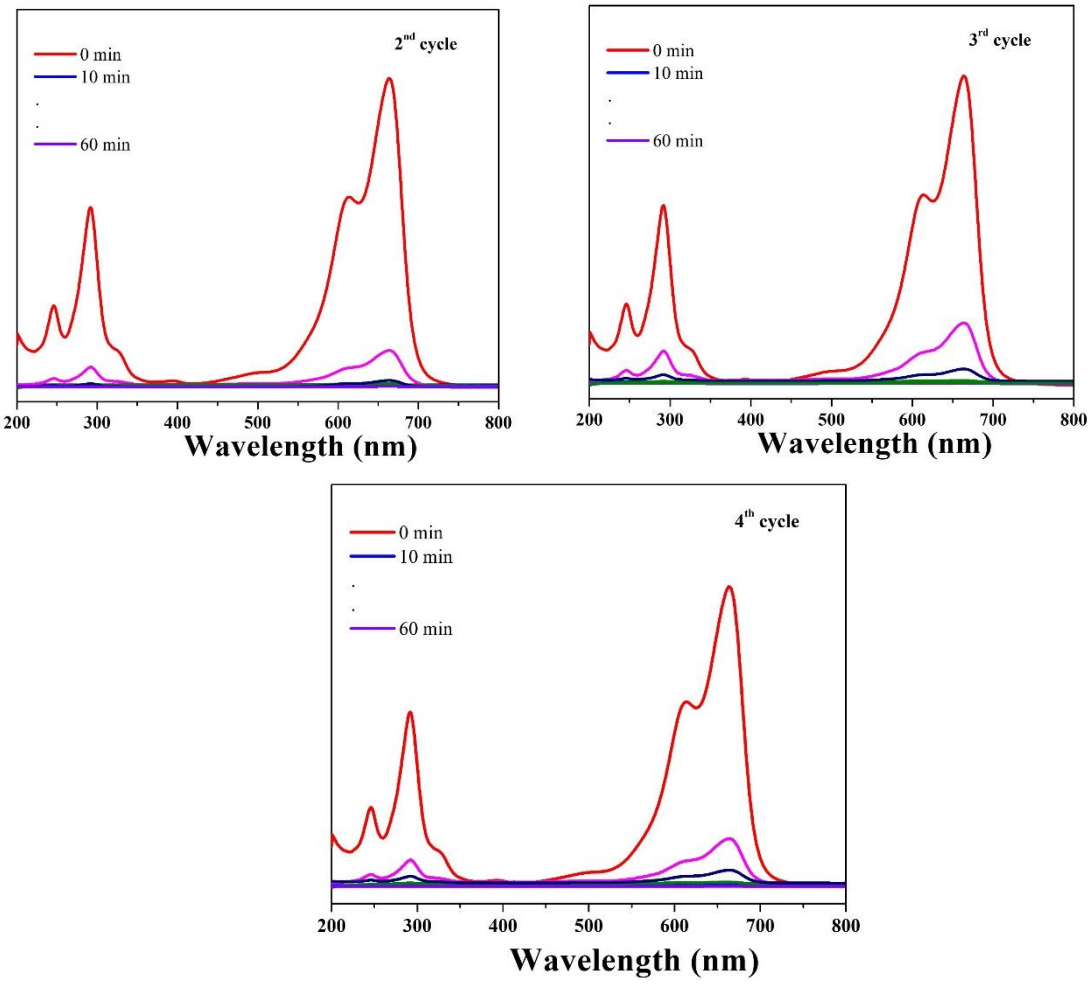

Figure S1. UV-Vis absorption spectra showing photodegradation of MB under sunlight irradiation for 4 cycles (1st cycle in the manuscript).

Figures

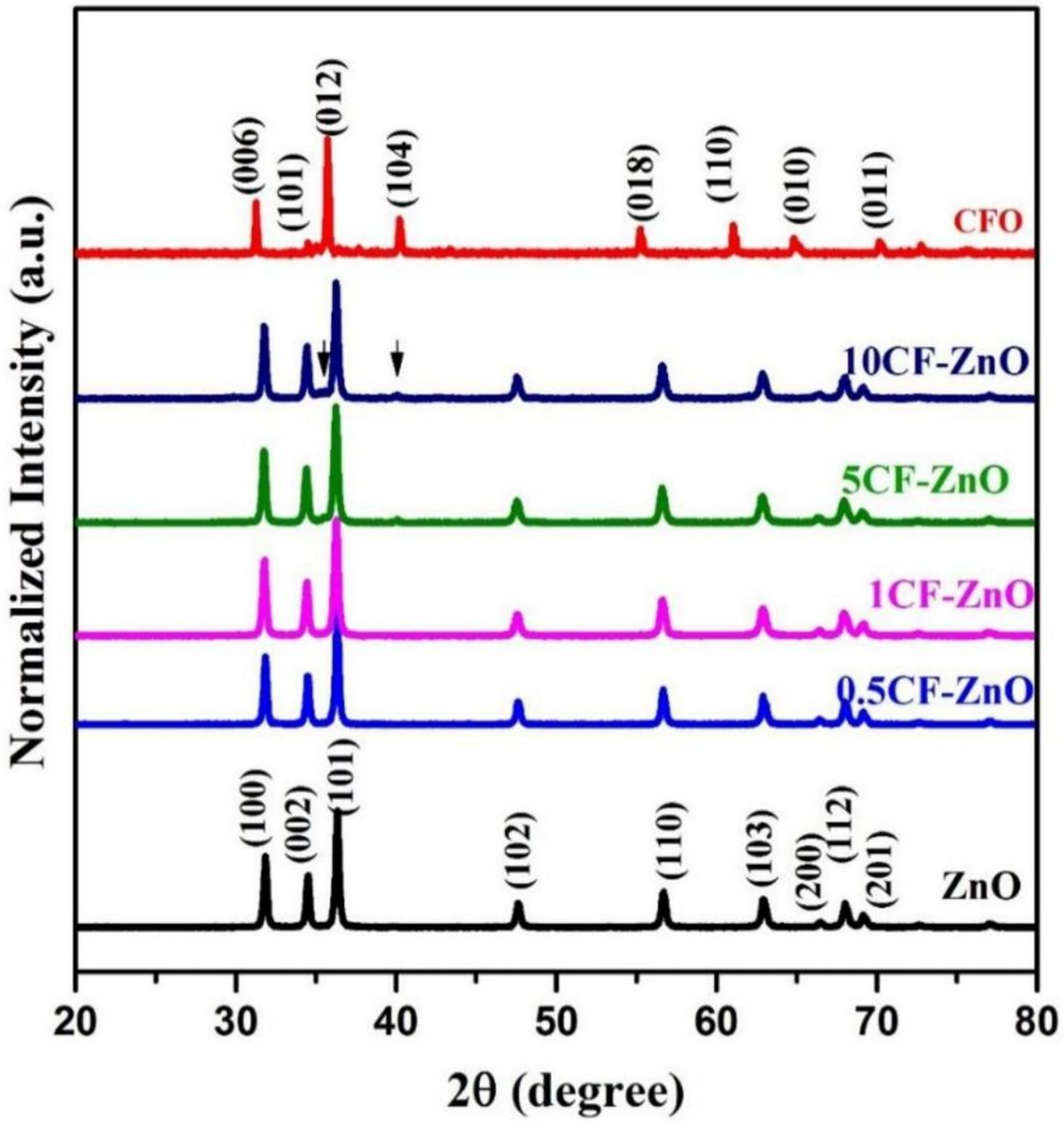

Figure 1

XRD pattern of pure ZnO, xCF-ZnO(x=0.5,1,5,10) and pure CFO. The peaks marked with arrow corresponds to CuFeO2

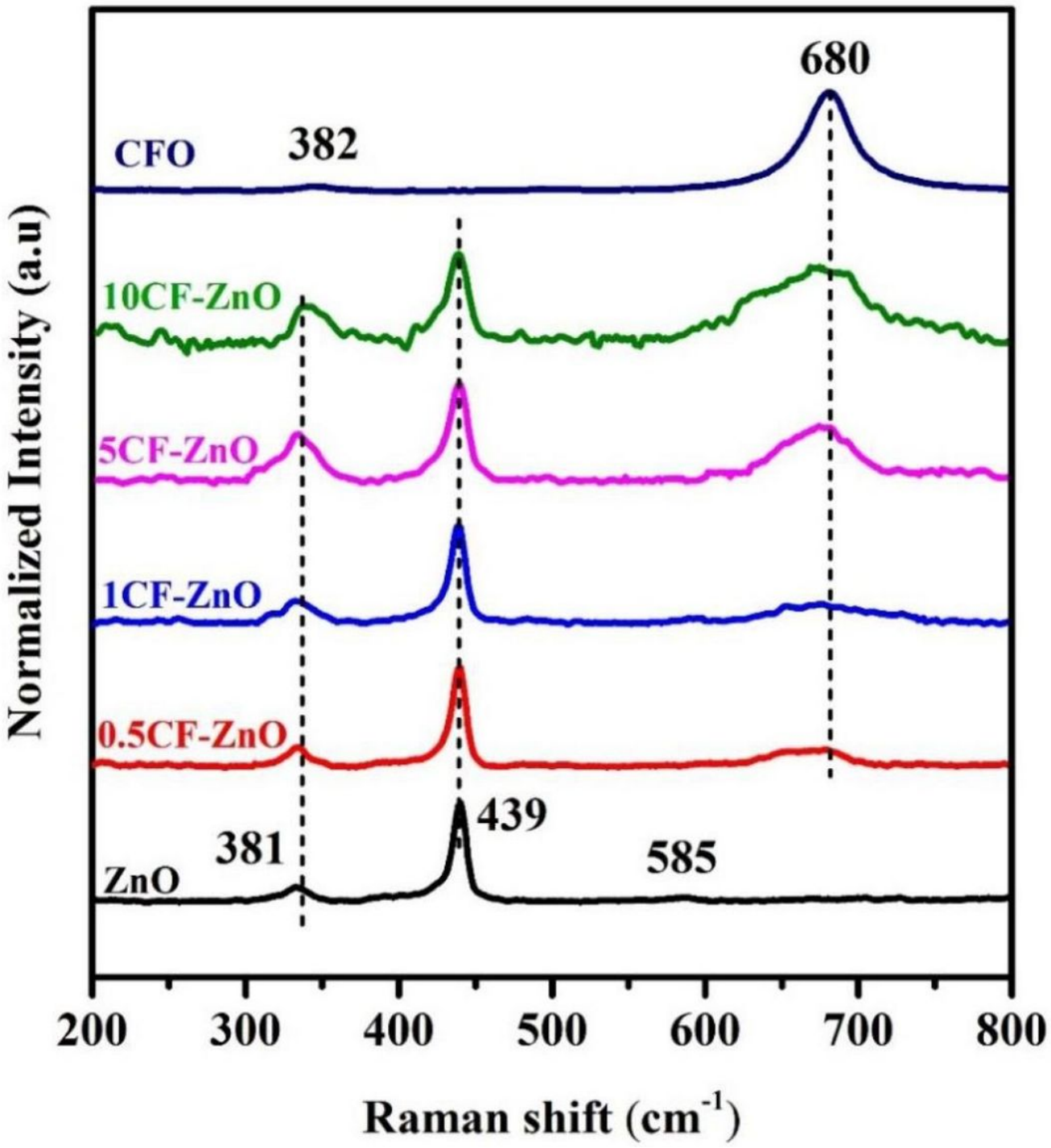

Figure 2

Raman spectra of ZnO, CFO and xCF-ZnO system

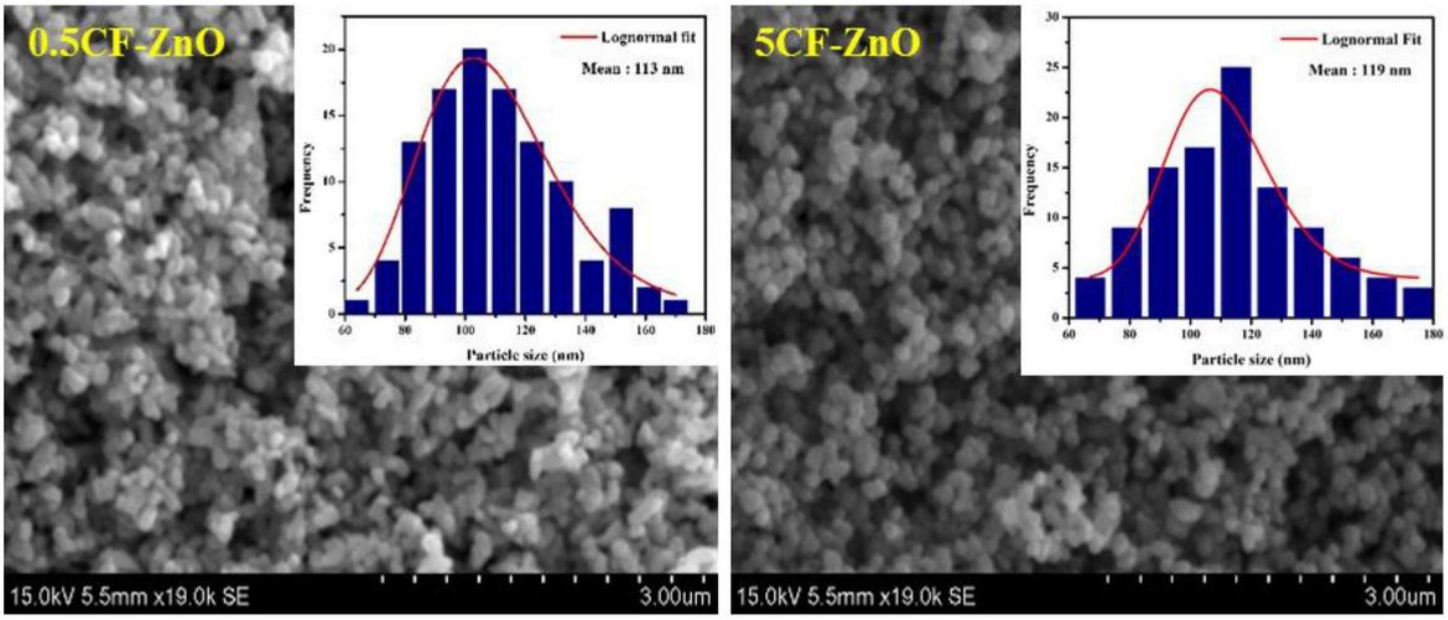

Figure 3

SEM images of 0.5CF-ZnO and 5CF-ZnO

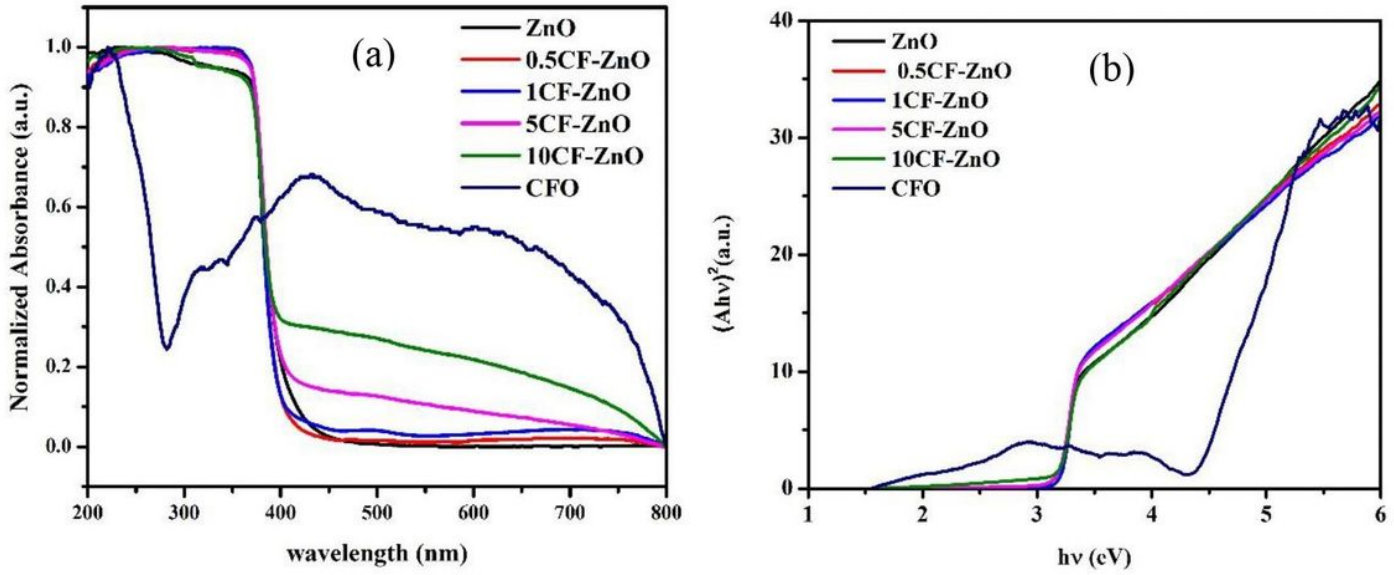

Figure 4

Absorbance spectra (a) Tau plot (b) of the xCF-ZnO system

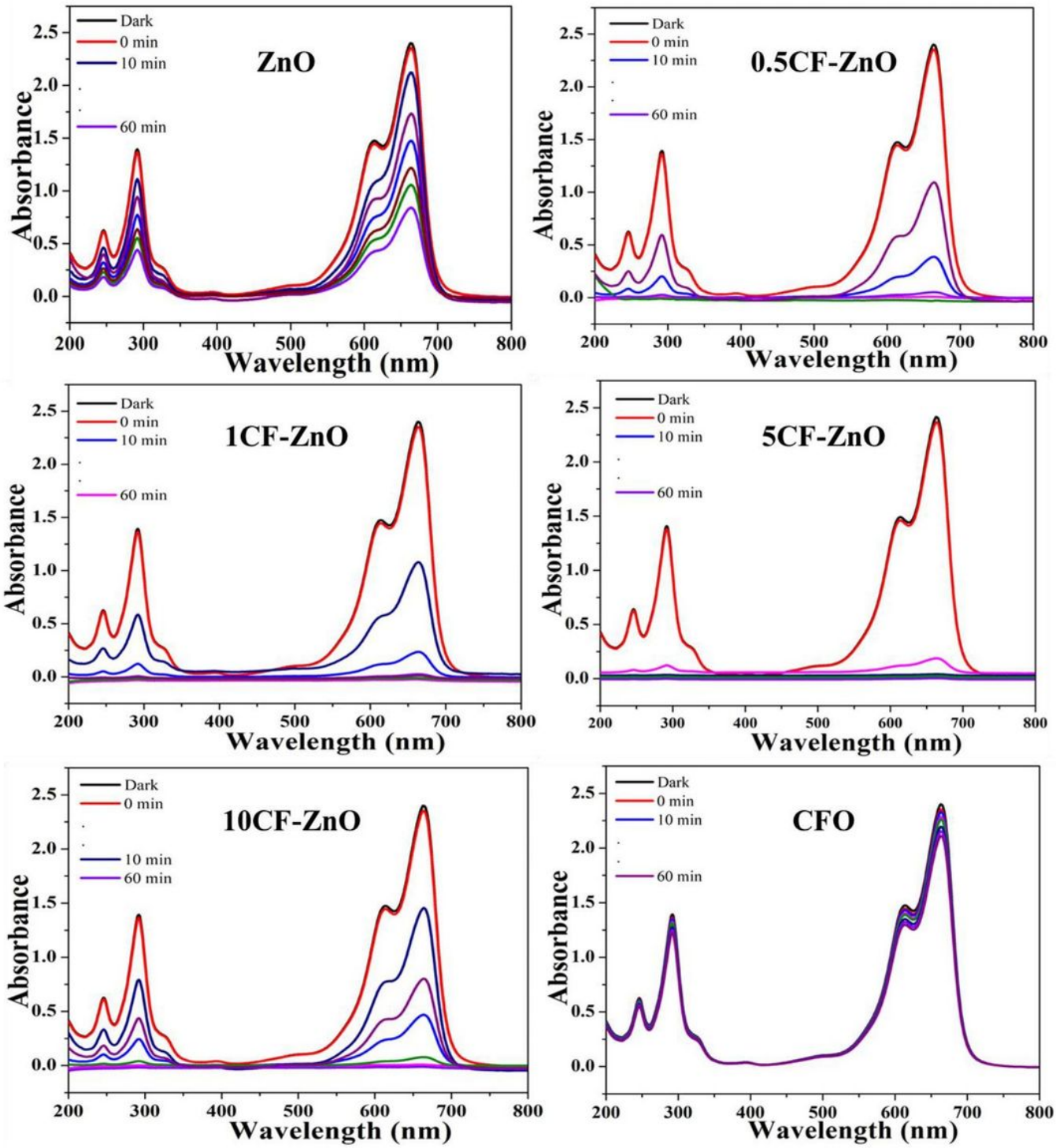

Figure 5

Absorption spectra for the degradation of methylene blue by sunlight for ZnO and xCFZnO system

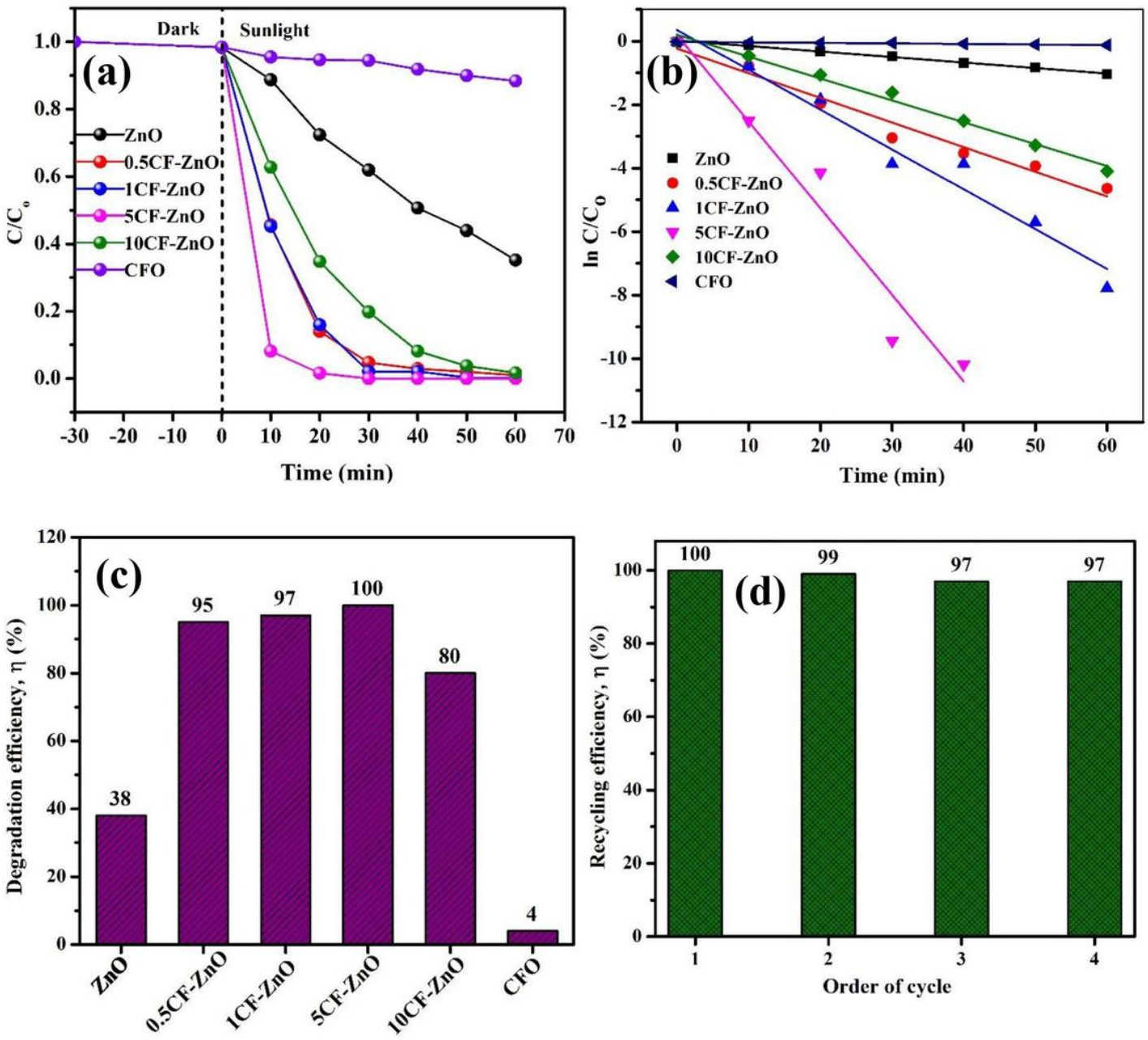

Figure 6

a) Concentration vs irradiation time profile b) Reaction kinetics c) degradation efficiency at 30 min of ZnO and xCF-ZnO system for the degradation of methylene blue d) degradation efficiency of 5CF-ZnO for consecutive 4 cycles at 30 min

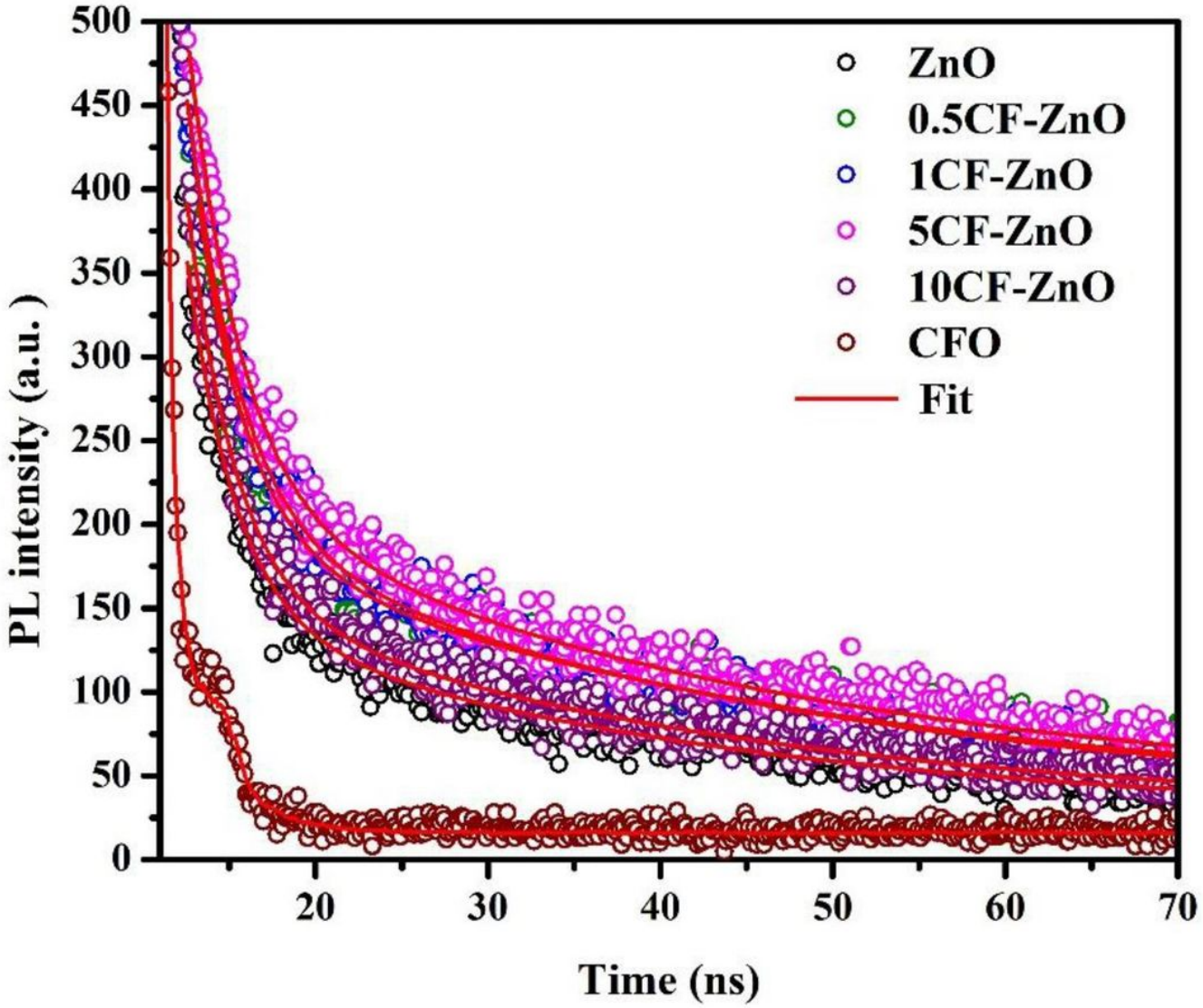

Figure 7

Time resolved photoluminescent decay of pure ZnO,CFO and xCF-ZnO heterostructures

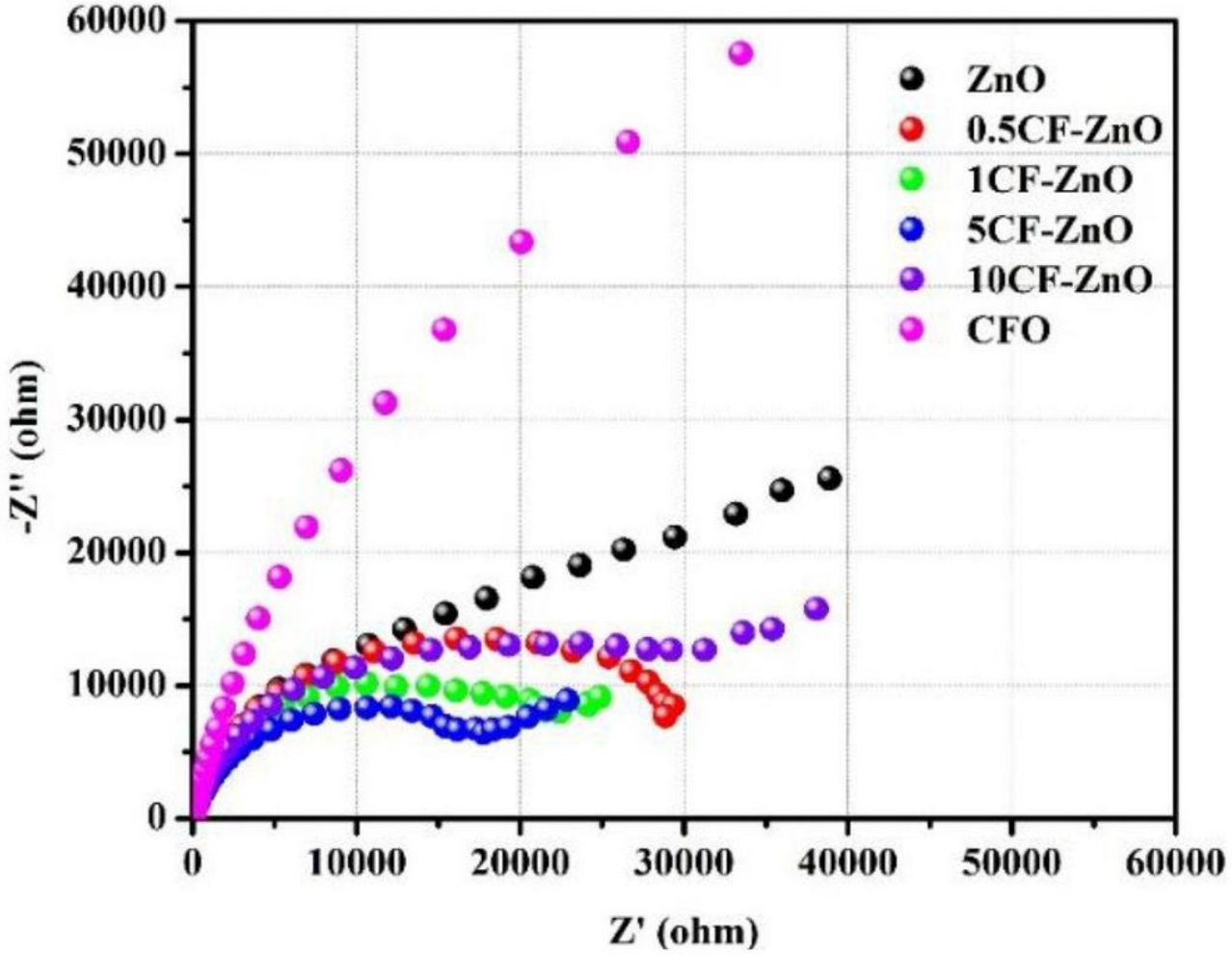

Figure 8

Nyquist plot and Mott Schottky plot of xCF-ZnO system

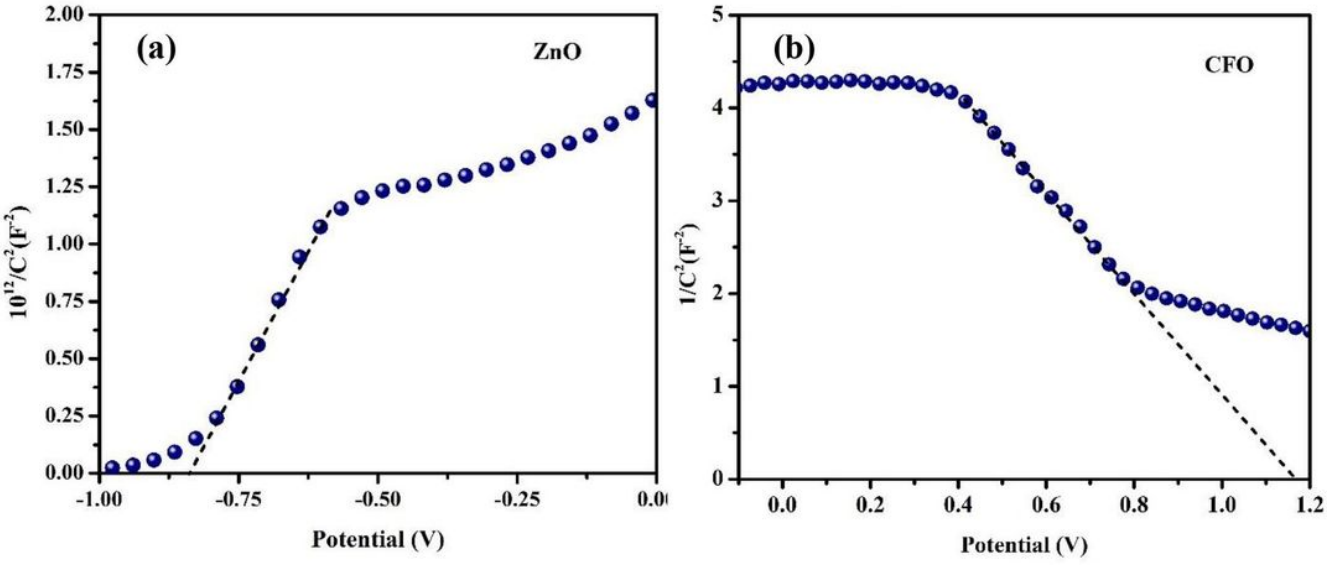

Figure 9

Mott-Schottky plots of (a) ZnO and (b) CuFeO2.

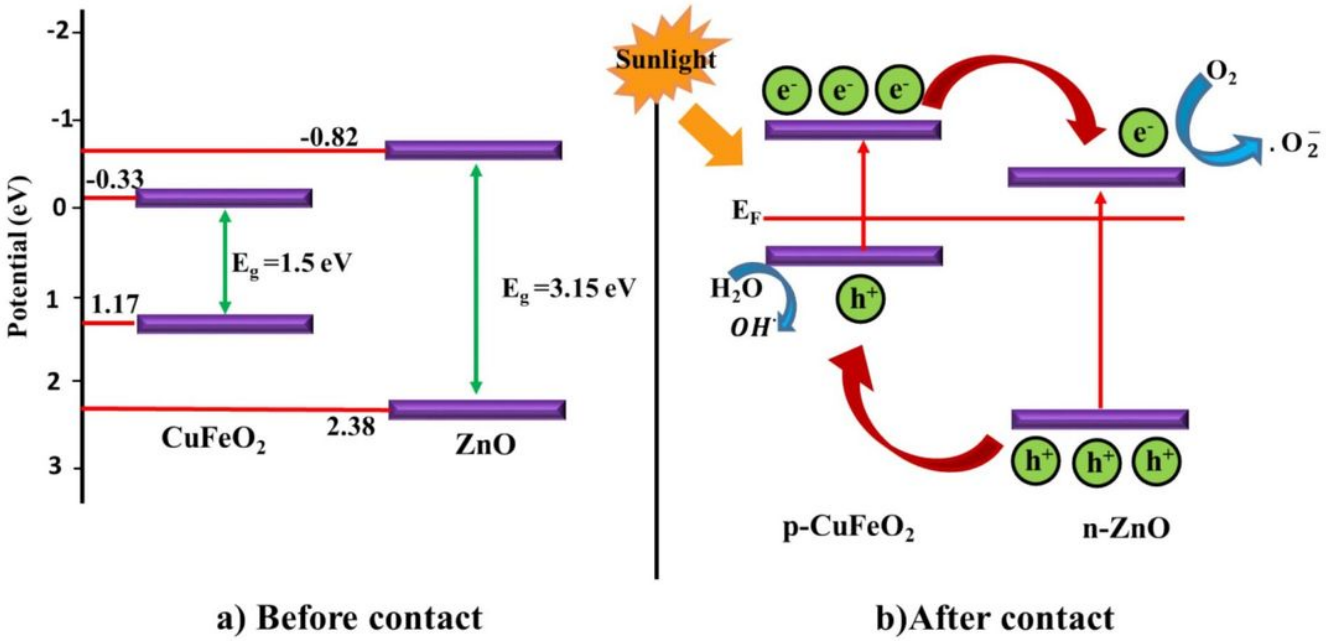

Figure 10

Schematic diagram for the photocatalytic mechanism of CF-ZnO heterostructures